CONFERENCE PRE-PRINT

CORE-EDGE INTEGRATION STUDIES IN NEGATIVE TRIANGULARITY IN TCV

O. FÉVRIER, G. DURR-LEGOUPIL-NICOUD, C. CONTRÉ, R. MORGAN, O. SAUTER, C. THEILER, S. CODA, A. PEREK, H. REIMERDES, E. TONELLO, B. VINCENT, M. ZURITA

Ecole Polytechnique Fédérale de Lausanne (EPFL), Swiss Plasma Center (SPC)

Lausanne, Switzerland

Email: olivier.fevrier@epfl.ch

F. MOMBELLI, A. MASTROGIROLAMO, M. PASSONI Politecnico di Milano, Department of Energy Milan, Italy

The TCV team^a and the EUROfusion Tokamak Exploitation Team^b

^aSee the author list of B.P. Duval et al 2024 *Nucl. Fusion* **64** 112023.

Abstract

In this contribution, we demonstrate the core-edge integration of negative triangularity (NT) plasmas with reactor-relevant operation. High input power scenarios are developed employing the Neutral Beam Injection (NBI) system of TCV, achieving high performance, with β_N up to 1.7 ($H_{98,y2}$ above 1), at a relatively high density (Greenwald fraction of approximately 0.4, vs 0.55 for the positive triangularity (PT) H-Mode) sustained under stationary conditions, for the duration of the NBI. The NT scenario achieves central ion and electron temperatures that are higher than those of its PT counterpart. Before any extrinsic impurity seeding, the divertor is already relatively cold, as evidenced by the CIII front retreating from the outer target, a low outer target temperature ($T_e \approx 6$ eV) and a significant radiated power fraction, attributed in part to the high operational density. With divertor N_2 seeding, an X-Point Radiator is formed, further cooling the divertor, with only a slight reduction in plasma performance.

1. INTRODUCTION

Future tokamak fusion reactors are predominantly designed to operate in the High-confinement mode (H-mode). In this regime, an edge transport barrier leads to the formation of a temperature and density pedestal, resulting in a doubling of the energy confinement time compared to the Low-confinement mode (L-mode), for otherwise identical parameters.

Unfortunately, H-mode operation introduces significant challenges. Accessing and sustaining H-mode requires the power crossing the separatrix to be above a certain threshold, constraining the operational space, especially regarding the power that can be radiated in the plasma core. Furthermore, this threshold can currently only be estimated through extrapolations from existing experiments, leading to large extrapolation uncertainties. In addition, the high power crossing the separatrix poses a severe challenge for power exhaust. When combined with the characteristically narrow Scrape-Off Layer (SOL) width (λ_q) of H-mode [1], projected divertor target power loads in reactors like ITER and DEMO will far exceed material limits if left unmitigated [2]. Consequently, operation in a detached divertor regime is considered mandatory for a fusion power plant [3, 4]. An additional drawback of the H-mode regime is the presence of Edge Localized Modes (ELMs), instabilities of the pedestal leading to intense transient heat loads on divertor targets. Unmitigated, ELMs will lead to unacceptable heat loads on the divertor components, and possibly partial melting, and therefore must be suppressed [4]. Although operating in a detached divertor state may partially mitigate ELMs' energy, and dedicated ELM-free scenarios are under development, handling these events remains a critical obstacle [5].

The Negative Triangularity (NT) configuration has emerged as a leading alternative to the standard H-Mode operation, due to its ability to achieve H-mode-grade confinement while operating in L-mode. This was first observed in the TCV tokamak [6, 7], where the enhanced energy confinement is attributed to a significant reduction in plasma turbulence levels [8]. The achievement of high L-mode confinement in NT has since been demonstrated

^bSee the author list of E. Joffrin et al 2024 *Nucl. Fusion* **64** 112019.

in other devices. In DIII-D, NT L-mode discharges with $\beta_N = 2.7$ and $H_{98,y2} = 1.2$ [9] were achieved, while AUG has also reported high energy confinement in electron-heated NT plasmas [10]. Since the NT scenarios operate in L-Mode, they do not feature any pedestal at the edge of the confined region, and are therefore ELMfree. However, the integration of NT with a robust power exhaust solution remains an active area of research. Ohmic experiments on TCV have shown that achieving divertor detachment is significantly more challenging in NT configurations compared to positive ones [11]. Likewise, on DIII-D, while detachment was reached in NBI-heated discharges with reactor-relevant performance ($H_{98,y2} \approx 1, \beta_N \approx 2$), it required higher densities than in equivalent positive triangularity plasmas, a result partially linked to geometrical effects [12]. Increasing divertor closure in TCV helps to further cool the outer target, but the relative difficulty of reaching detachment compared to PT remains, and strong detached Ohmic lower-single-null NT plasmas could not be achieved with core density ramp alone [13]. Moreover, measurements over a large dataset of TCV discharges revealed that λ_q also narrows as the upper triangularity becomes more negative [14]. This is consistent with the challenges in accessing detachment. Further experiments in TCV have shown that detachment can be induced with impurity seeding, albeit at the cost of confinement degradation, which is, however, not found to be more severe than in comparable impurity seeded PT discharges [11, 15]. This work demonstrates the development of a highperformance, stationary negative triangularity L-mode scenario that achieves energy confinement comparable to H-mode and is compatible with a fully detached divertor, establishing it as an attractive, ELM-free regime for a future fusion reactor.

This paper is organized as follows. Section 2 presents the experimental setup. In Section 3, the scenarios developped for this study, and their performances, are described, and Section 4 compares their divertor performances. Finally, conclusions are presented in Section 5.

2. EXPERIMENTAL SETUP

This work has been performed on the TCV tokamak (major radius $R_0 = 0.88$ m, minor radius a = 0.24 m, $B_0 = 0.88$ 1.44 T). This study focuses on diverted NBI (Neutral Beam Injection)-heated L-mode NT configurations, which are compared to diverted NBI-heated L- and H-mode PT configurations. Herein we distinguish between the upper (or top) triangularity, δ_u , and the bottom (or lower) triangularity, δ_l . Figure 1a shows the magnetic geometries used in this study together with the location of the gas valves (black rectangles) and the spatial coverage of the diagnostics most relevant for this work. D2 is injected through the outermost valves at a fueling rate controlled by a feedback loop based on the line-averaged density $\langle n_e \rangle_{FIR}$ measured by a vertical chord ($R=0.9~\mathrm{m}$) of the FIR (Far-InfraRed interferometer). N₂ is injected through the innermost valve, following a prescribed ramp. The locations of the wall-embedded Langmuir Probes (LPs) [16, 17] are indicated by green dots. The black squares indicate the locations of the Thomson Scattering (TS) measurements [18]. These measurements are used to compute $\langle n_e \rangle$, defined as the integral of the density inferred by TS within the LCFS, divided by the height of the plasma core at R=0.9 m, [11]. Not shown in Figure 1a is the multi-spectral imaging diagnostic MANTIS (Multispectral Advanced Narrowband Tokamak Imaging System) [19]. The images captured by MANTIS are tomographically inverted to obtain two-dimensional poloidal maps of the emissivity of the selected radiation lines. In particular, in this paper, we will focus on the CIII (465.8 nm) line emissions. In the following, the radial coordinate ρ_{ψ} is the normalized poloidal magnetic flux, defined as $\rho_{\psi} = \sqrt{(\psi - \psi_0)/(\psi_1 - \psi_0)}$ where ψ is the poloidal magnetic flux, with ψ_0 and ψ_1 the flux at the magnetic axis and at the primary X-point, respectively.

3. TOWARDS HIGH-PERFORMANCE, FULLY DETACHED NT SCENARIOS

The experiments were carried out with a plasma current (I_p) of 170 kA, a typical value for H-Mode discharges in TCV. The ion ∇B -drift is directed towards the X-Point, favorable for H-Mode access. The discharges were all NBI-heated. In these experiments, TCV was equipped with the "SILO" version of its divertor gas baffles [20, 21], leading to a closed divertor, Fig. 1a. A significant operational challenge in the development of the NT scenario was density control. The core fueling provided by NBI, combined with favorable confinement conditions, often leads to an uncontrolled rise in the core plasma density. This, in turn, enhances the NBI power coupling, leading to a rapid increase in β_N that ultimately culminates in a disruption. To avoid this, the NBI power in the NT configuration is slowly ramped-up from the minimum achievable starting power ($\approx 210 \text{ kW}$) to its final value (750 kW for the scenario discussed in this work). Attempts to extend to higher NBI power were unsuccessful due to the loss of density control. Ultimately, the developed NT L-Mode scenario has a negative upper triangularity ($\delta_u = -0.29$, Fig. 1a), a positive lower triangularity ($\delta_l = 0.45$) with 750 kW of NBI, Fig. 1c, and density $\langle n_e \rangle \approx 4.3 \times 10^{19} \text{ m}^{-3}$, Fig. 1b. The performance of the NT L-Mode scenario is benchmarked against two distinct reference scenarios. First, a PT L-Mode, with a positive upper triangularity ($\delta_u = 0.19$, Fig. 1a) with 750 kW of NBI, Fig. 1c, and density $\langle n_e \rangle \approx 3.25 \times 10^{19} \text{ m}^{-3}$, Fig. 1b, and, being L-Mode, no ELMs, as seen by the

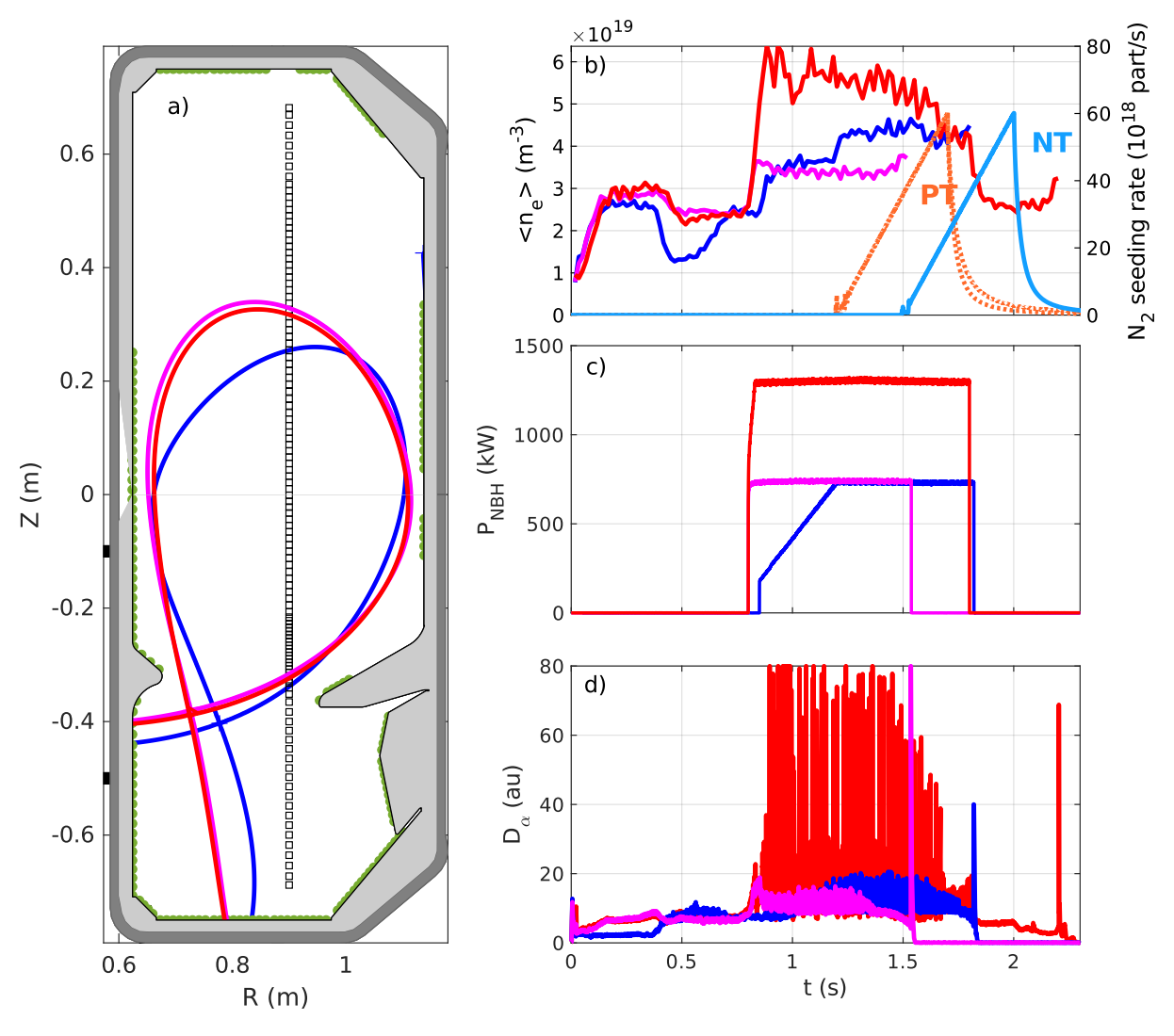


FIG. 1. (a) (blue) NT equilibrium ($\delta_{top} \approx -0.29$, $\delta_{bot} \approx 0.45$) (magenta and red) PT equilibria ($\delta_{top} \approx 0.19$, $\delta_{bot} \approx 0.7$). The green dots correspond to the positions of the Langmuir Probes. The black squares correspond to the locations of the measurement points of the Thomson Scattering system. (right panels) Time evolution of the (b) (left axis) core line-averaged density $\langle n_e \rangle$ from TS, (c) NBI auxiliary power (injected to the plasma), and (d) D- α , measured by a photo-diode, for the NT L-Mode case (blue), PT L-Mode case (magenta) and the PT H-Mode case (red), summarized in Table 1. (b) (right axis) N₂-seeding rate for the NT (light blue) and PT (orange) cases.

quiescent D_{α} signal, Fig. 1d. Second, a PT H-Mode, with a positive upper triangularity ($\delta_u=0.19$) with 1.3 MW of injected NBI power, Fig. 1c, a density $\langle n_e \rangle \approx 5-6 \times 10^{19}~{\rm m}^{-3}$, Fig. 1b, and ELMs clearly visible on the D_{α} signal, Fig. 1d. This discharge is characterized by the onset of a large m/n = 2/1 tearing mode, causing a significant degradation of confinement, as will be discussed later. Consequently, performance comparisons are restricted to the time window preceding the onset of this instability. With N_2 -seeding, the ELMs' amplitude decreases, until they ultimately disappear (at $t\approx 1.6~{\rm s}$). H-Mode is only lost at $t\approx 1.8~{\rm s}$ when the NBI is switched off. In all scenarios, a feed-forward programmed N_2 -seeding ramps start either at $t=1.25~{\rm s}$ (PT) or $t=1.5~{\rm s}$ (NT). Table 1 lists the discharges used in this study. It should be noted that the discharge of the NT L-mode itself exhibits a weak m/n = 2/1 mode, which is estimated to reduce confinement by up to 15%. We further remark here that the goal of this study is not to establish the NT configuration as a performance record-breaking contender. Rather, the goal is to show that the NBI-heated NT L-Mode can reach performances that are close to that of an H-Mode plasmas.

Label	Discharge	δ_u	δ_l	NBI power	$\langle n_e \rangle \ (\times 10^{19} \ \mathrm{m}^{-3})$	N ₂ -seeding starting time (s)
NT L-Mode	83686	-0.29	0.45	750 kW	≈ 4.3	1.5s
PT L-Mode	83824	0.19	≈ 0.7	750 kW	≈ 3.25	1.25s
PT H-Mode	83834	0.19	≈ 0.7	1.3 MW	$\approx 5-6$	1.25s

TABLE 1. SUMMARY OF THE PLASMA DISCHARGES USED IN WORK, WITH MAIN RELEVANT PLASMA PARAMETERS.

With 750 kW of NBI-heating power, the NT L-Mode achieves $\beta_N \approx 1.7$ in a stationary phase, while the PT L-Mode achieves only $\beta_N \approx 1.2$, 40% lower than the NT, Figure 2a. The PT H-Mode, with 1.3 MW of NBI, initially achieves $\beta_N \approx 2.1$, 25% higher than the NT L-Mode (but with 73% higher injected power), that drops to $\beta_N \approx 1.55$ due to the onset of a 2/1 tearing mode. To further compare the three scenarios, accounting for the variation in parameters (density, injected power, etc.), we also evaluate and compare the confinement enhancement factor, $H_{98,y2}$, Figure 2b, that quantifies how the confinement time compares to that expected from the ITER98y2 scaling law [22]. As expected, the PT L-Mode exhibits the lower $H_{98,y2} \approx 0.8 - 0.9$. The PT H-mode initially exhibits $H_{98,y2} \approx 1.4$, until the onset of a 2/1 tearing mode, which reduces $H_{98,y2}$ to ≈ 1 , further dropping later in the discharge due to N₂-seeding, to $H_{98,y2}$ to approximately 0.9. The NT L-Mode clearly achieves the highest $H_{98,y2}$, approximately 1.3, of all scenarios, maintained from t=1.2 s to t=1.5 s. We remark here that, using $H_{98,y2}$ as the comparison metrics, the NT L-Mode matches the 2/1-free PT H-Mode within less than 10%. After t=1.5 s, $H_{98,y2}$ drops slightly, due to the combined effect of a weak m/n = 2/1 mode and N₂-seeding, although it is difficult to establish if the 2/1 appearance is linked to the N₂ seeding.

The periodic drops observed in $H_{98,y2}$ in NT correspond to times at which 500 kW blips of the second Neutral Beam injector of TCV, NBI2, were performed, to enable Charge eXchange Recombination Spectroscopy (CXRS), due to the unavailability of the Diagnostic Neutral Beam injector (DNBI, 100 kW) that was used in the PT L- and H-Modes. We note, however, that even during these events, $H_{98,y2}$ remains above 1.1. To summarize, the NT L-Mode achieves similar peak $H_{98,y2}$ as the PT H-Mode, with only 25% lower peak β_N (2.1 vs 1.7) than the PT H-Mode, with 42% lower injected heating power (1.3MW vs 750 kW).

To support the observations on β_N and $H_{98,y2}$, we now turn to kinetic profiles (electron density, electron and ion temperatures), measured with either TS (for electrons) or CXRS (for ions). The NT L-Mode is characterized by higher electron temperature, Figure 3a, and ion temperature, 3d, than the PT H-Mode, and higher electron temperature, Figure 3a, and a central ion temperature comparable to that of the PT L-Mode, Figure 3d. However, in the case of the PT H-Mode, this can be ascribed to the lower $\langle n_e \rangle$ of the

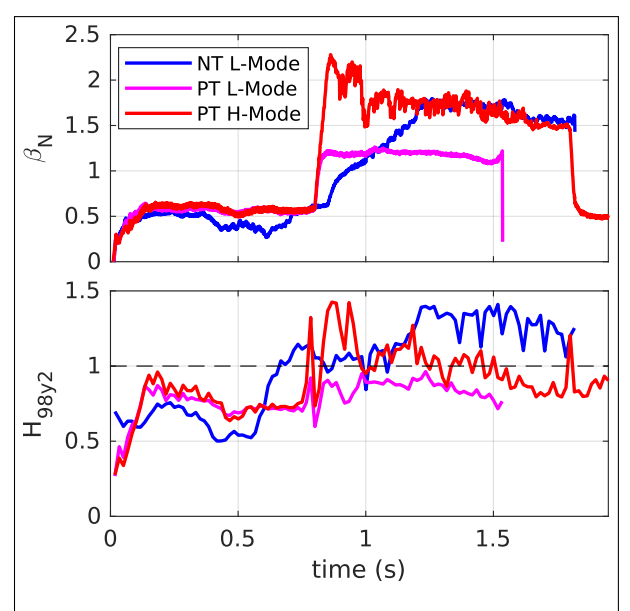


FIG. 2. (a) β_N and (b) $H_{98,y2}$ as a function of time for the discharges listed in Table 1

NT L-Mode, Figure 1b and Figure 3b, and, to some extent, to the 2/1-tearing mode present in the PT H-Mode

(and clearly visible by the flattening of the electron temperature near $\rho_{\psi}\approx 0.55$, Figures 3a and 3c). Electron pressures are, however, similar in the NT L-Mode and in the PT H-Mode (before the triggering of the MHD mode) in the core plasma ($\rho_{\psi} \leq 0.6$), although slightly lower in the very core for the NT L-Mode, Figure 3c. In the edge region, a clear electron density and temperature pedestal is visible in the PT H-Mode, as expected, whereas no such pedestal is observed in the NT L-Mode, whose edge behaves more similarly to that of the PT L-Mode, except for a generally stronger T_e gradient over the entire profile. Taken together, the inferred β_N and $H_{98,y2}$ and the kinetic profiles support the interpretation that the NT L-Mode scenario is closer, in terms of core performances, to that of the PT H-Mode.

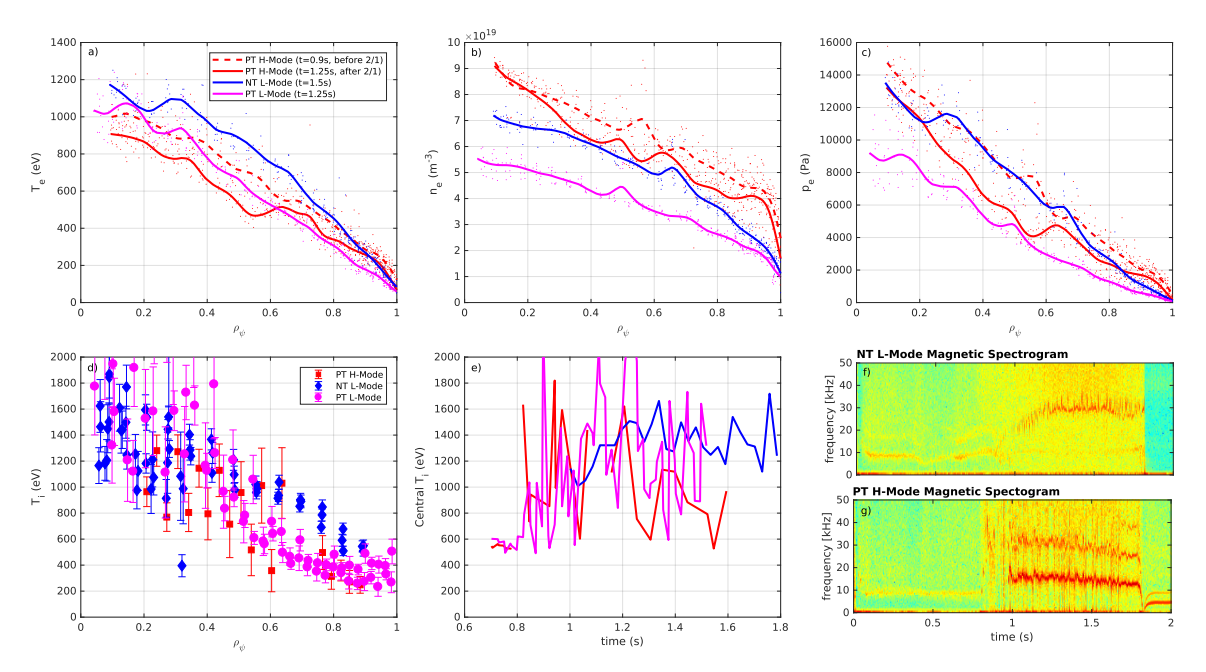


FIG. 3. Core profiles as a function of ρ_{ψ} of electron temperature (a), density (b) and pressure (c), measured by TS, for the discharges used in this study, Table 1, before N_2 -seeding. For the PT H-Mode, the profiles before (dahsed lines) and after (solid lines) the onset of a strong 2/1 tearing mode are shown. (d) Core profiles as a function of ρ_{ψ} of the ion temperature, measured by CXRS, before N_2 -seeding. (e) Time evolution of the central ion temperature. (f-g) Spectrogram of magnetic field fluctuations for the NT L-Mode (f) and the PT H-Mode (g).

4. ACHIEVING DETACHMENT IN HIGH-PERFORMANCES NT PLASMAS

In this section, we compare the NT and PT discharges from Table 1 from the point of view of power exhaust. We focus on the analysis of the outer target quantities, as measured by LP, before analyzing the radiative properties of these scenarios.

4.1. Evolution of outer target quantities

Shortly after the start of N_2 -seeding, the integrated particle flux to the outer target, Γ_t^o , drops in a similar way for the two considered L-Mode, Fig. 4a, a signature of detachment. A clear reduction of the peak electron temperature at the outer target T_e^{peak} is observed after the start of the N_2 -seeding in all cases, Fig. 4b. In H-Mode, a peak inter-ELM temperature of approximately 8 eV is observed before N_2 -seeding, that drops to approximately 5 eV before the loss of H-Mode. In the two L-Mode cases, NT and PT, which are heated with the same (injected) NBI power, we observe a similar initial T_e^{peak} of approximately 6 eV before N_2 seeding, dropping below 5 eV as N_2 is introduced. It may be surprising that the NT case features a target temperature similar to the PT case, considering that the former exhibits a higher $\langle n_e \rangle$ (and therefore a likely higher separatrix density), which would tend to reduce T_e^{peak} , all other quantities being kept the same. However, with different densities, the NBI coupling may differ between these two discharges. Furthermore, it is well established that λ_q is smaller in the NT compared to PT [23, 14]. The similar T_e^{peak} are likely the result of a complex interplay between these effects. Together, these observations show that with seeding N_2 , the three configurations ultimately detach.

4.2. Radiation distribution

We now employ a different indicator of detachment, the CIII emission location. Previous TCV studies showed that the position of the CIII emission along a divertor leg provides a convenient tool to assess the detached status of the divertor. Indeed, as the divertor cools, the CIII emission front moves away from the target towards the X-Point, acting as some sort of thermometer proxy [24, 21].

Even at the highest level of seeding, the H-Mode exhibits signs of reattachment during ELMs, Figure 5b and Figure 5d, with the CIII emission shooting back to the target. In between ELMs, the CIII emission moves up the leg, Figure 5a and Figure 5c, towards the X-Point, indicating detached inter-ELM phases, in agreement with LP measurements. This is further confirmed when performing tomographic inversions of the captured images, which show two clusters of points, Figure 5k, corresponding to images where the front is located either at the target (reattachment during ELM) and further up the outer leg (detachment between ELM).

This behavior is different in the NT plasma, where the CIII emission moves smoothly up the leg towards the X-Point as the N₂-seeding is increased, Figures 5a-j and Figure 5k, without transient reattachment due to ELMs. The PT L-Mode behaves similarly to the NT L-Mode. In both L-Mode cases, the CIII front is already away from the target even before N2-seeding, which is consistent with the low peak T_e measured by LP even before N2-seeding, ascribed to a combined role of the fairly high core density of these scenarios (due to NBI fueling) and the presence of the divertor baffles which facilitate access to detachment [20, 21]. In both L-Modes, bolometry shows that N2-seeding ultimately culminates in the formation of an X-Point Radiator [25], leading to only a small drop in terms of β_N and H_{98y2} for the NT L-Mode. Taken together, these observations confirm the achievement of a fully detached, X-point radiator, N2-seeded, NT L-Mode scenarios, with $\beta_N=1.5$ and $H_{98,y2}\approx 1.2-1.3$.

5. CONCLUSION

In this work, we have successfully developed a TCV NT L-mode scenario with auxiliary power (NBI) whose performance indicators are on par with those of a PT H-Mode scenario, in stationary conditions. These scenarios are compatible with detached divertor operation, with a modest reduction of confinement at the high level of detachment, possibly helped by the presence of the divertor baffles. This further establishes NT as an attractive regime for a reactor, combining good confinement with the quiescent edge of an L-Mode, thereby avoiding the challenges associated with ELMs and LH power threshold. In future work, these high-power scenarios will be further characterized with various sets of baffles, and extended to higher input power, using the TCV ECRH system, as

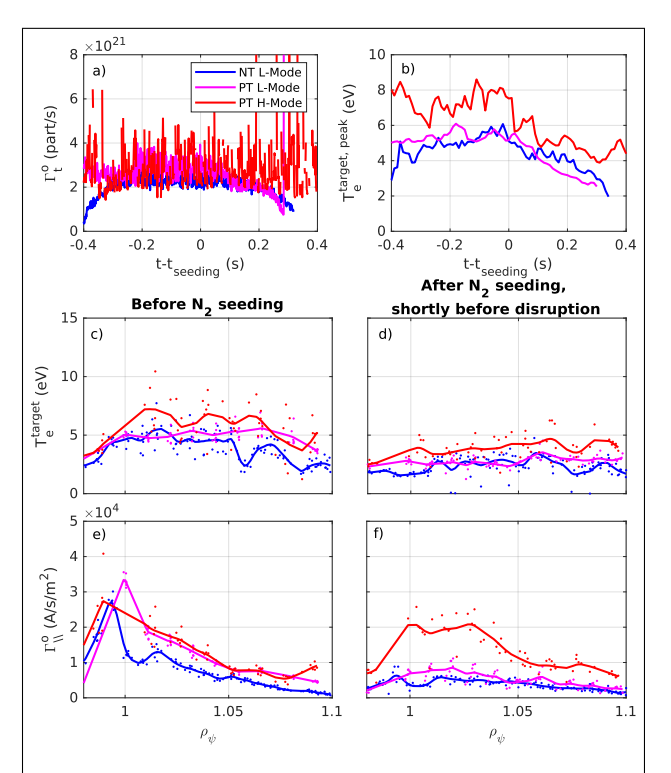


FIG. 4. (a) Evolution of the integrated particle flux to the outer target, Γ_e^t , and (b) of the outer target electron temperature, T_e^{peak} , as a function of time with respect to the start of N₂-seeding, for the NT L-Mode with 750kW of NBI (blue), the PT L-Mode with 750kW of NBI (magenta) and the PT H-Mode with 1.3MW of NBI. (c) Outer target electron temperature and (e) parallel particle flux profiles, as a function of ρ_{ψ} , before N₂-seeding. (d) Outer target electron temperature and (f) parallel particle flux profiles, as a function of ρ_{ψ} , shortly before disruption (or loss of H-Mode for the PT H-Mode), with N₂-seeding.

well as the second, higher energy, TCV NBI. The possibility of achieving even high-performance scenarios with a fully detached divertor, featuring either a radiative mantel or an X-Point Radiator, with extrinsic impurity seeding (N2, Ne, Ar) will be assessed.

ACKNOWLEDGEMENTS

This work has been carried out within the framework of the EUROfusion Consortium, partially funded by the European Union via the Euratom Research and Training Programme (Grant Agreement No 101052200 — EUROfusion). The Swiss contribution to this work has been funded by the Swiss State Secretariat for Education,

Research and Innovation (SERI). Views and opinions expressed are however those of the author(s) only and do not necessarily reflect those of the European Union, the European Commission or SERI. Neither the European Union nor the European Commission nor SERI can be held responsible for them. This work was supported in part by the Swiss National Science Foundation.

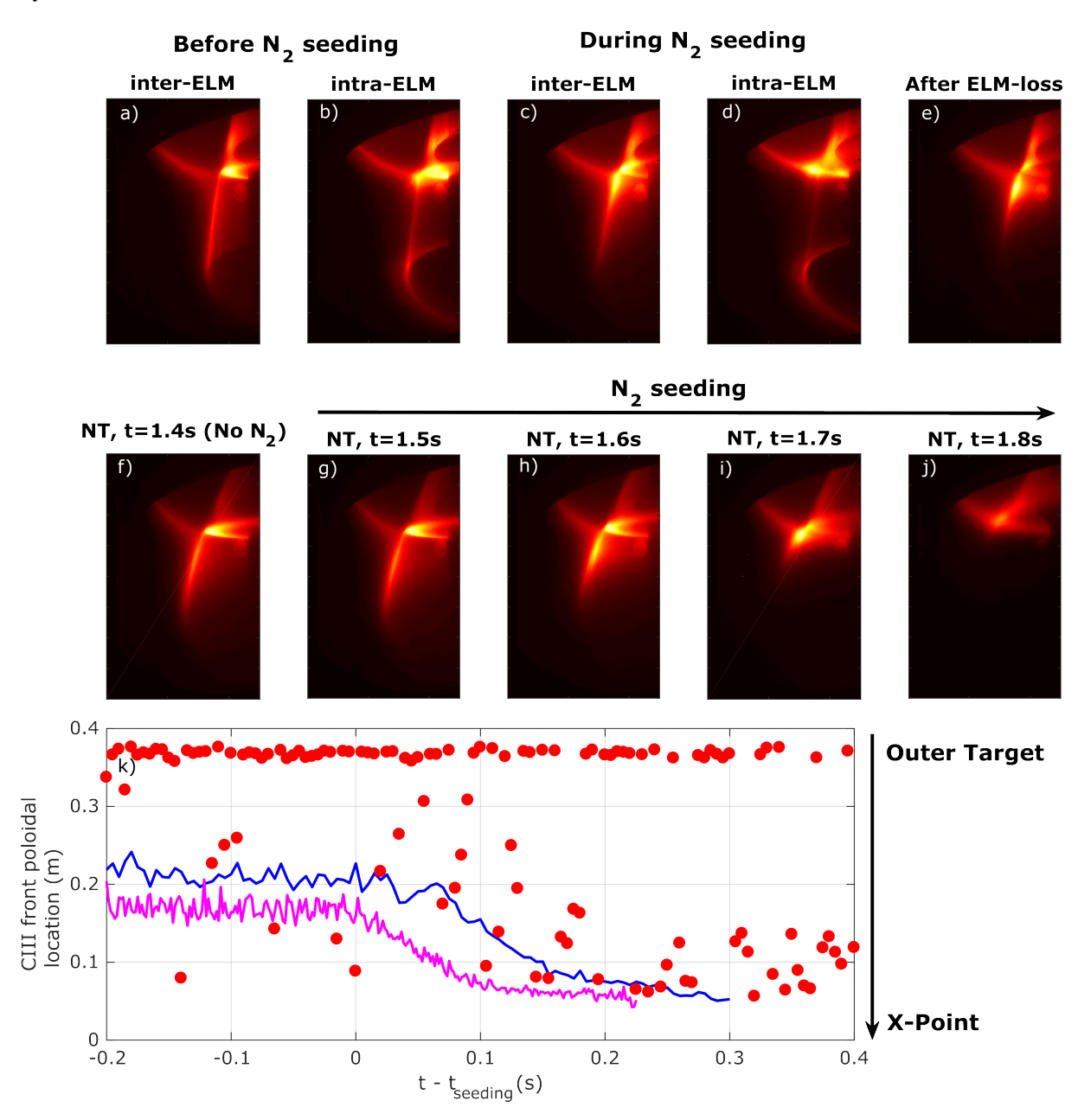


FIG. 5. (a-e) MANTIS CIII images taken during the PT H-Mode discharges before N_2 seeding (a-b), between ELMs (a) and during an ELM (b), during N_2 seeding (c-d), between ELMs (c) and during an ELM (d), and after the loss of ELMs (e). (f-j) MANTIS CIII images taken during the NT L-Mode discharges before N_2 -seeding (f) and at various times during N_2 -seeding (g-j). (k) Evolution of the CIII front poloidal location as a function of time with respect to N_2 -seeding for the discharges considered in this work. The color code is identical to that of Figure 4.

REFERENCES

- [1] EICH, T., LEONARD, A., PITTS, R., et al., "Scaling of the tokamak near the scrape-off layer H-mode power width and implications for ITER", *Nucl. Fusion*, **53** 9 (2013) 093031.
- [2] REIMERDES, H., AMBROSINO, R., INNOCENTE, P., et al., "Assessment of alternative divertor configurations as an exhaust solution for DEMO", *Nucl. Fusion*, **60** 6 (2020) 066030.

- [3] LEONARD, A. W., "Plasma detachment in divertor tokamaks", *Plasma Phys. Controlled Fusion*, **60** 4 (2018) 044001.
- [4] PITTS, R., BONNIN, X., ESCOURBIAC, F., et al., "Physics basis for the first ITER tungsten divertor", *Nucl. Mater. Energy*, **20** (2019) 100696.
- [5] VIEZZER, E., AUSTIN, M., BERNERT, M., et al., "Prospects of core–edge integrated no-ELM and small-ELM scenarios for future fusion devices", *Nucl. Mater. Energy*, **34** (2023) 101308.
- [6] POCHELON, A., GOODMAN, T., HENDERSON, M., et al., "Energy confinement and MHD activity in shaped TCV plasmas with localized electron cyclotron heating", *Nucl. Fusion*, **39** 11Y (1999) 1807.
- [7] CAMENEN, Y., POCHELON, A., BEHN, R., et al., "Impact of plasma triangularity and collisionality on electron heat transport in TCV L-mode plasmas", *Nucl. Fusion*, **47** 7 (2007) 510.
- [8] FONTANA, M., PORTE, L., CODA, S., et al., "Effects of collisionality and Te/Ti on fluctuations in positive and negative delta tokamak plasmas", *Nucl. Fusion*, **60** 1 (2019) 016006.
- [9] AUSTIN, M. E., MARINONI, A., WALKER, M. L., et al., "Achievement of Reactor-Relevant Performance in Negative Triangularity Shape in the DIII-D Tokamak", *Phys. Rev. Lett.* **122** (2019) 115001.
- [10] HAPPEL, T., PÜTTERICH, T., TOLD, D., et al., "Overview of initial negative triangularity plasma studies on the ASDEX Upgrade tokamak", *Nucl. Fusion*, **63** 1 (2022) 016002.
- [11] FÉVRIER, O., TSUI, C. K., DURR-LEGOUPIL-NICOUD, G., et al., "Comparison of detachment in Ohmic plasmas with positive and negative triangularity", *Plasma Phys. Controlled Fusion*, **66** 6 (2024) 065005.
- [12] SCOTTI, F., MARINONI, A., MCLEAN, A., et al., "High performance power handling in the absence of an H-mode edge in negative triangularity DIII-D plasmas", *Nucl. Fusion*, **64** 9 (2024) 094001.
- [13] DURR-LEGOUPIL-NICOUD, G., FÉVRIER, O., THEILER, C., et al. In preparation.
- [14] MORGAN, R. I., DURR-LEGOUPIL-NICOUD, G., FÉVRIER, O., et al., "Triangularity dependence of the divertor heat flux profile and SOL filamentary turbulence on TCV", *Nucl. Fusion* (2025).
- [15] DURR-LEGOUPIL-NICOUD, G., "Studying the Role of Divertor Closure and N2 Detachment in NT L-Mode plasmas on TCV", P.495, paper presented at the 50th EPS Conference on Plasma Physics, 2024.
- [16] FÉVRIER, O., THEILER, C., DE OLIVEIRA, H., et al., "Analysis of wall-embedded Langmuir probe signals in different conditions on the Tokamak à Configuration Variable", *Rev. Sci. Instrum.* **89** 5 (2018) 053502.
- [17] DE OLIVEIRA, H., MARMILLOD, P., THEILER, C., et al., "Langmuir probe electronics upgrade on the Tokamak à Configuration Variable", *Rev. Sci. Instrum.* **90** 8 (2019) 083502.
- [18] ARNICHAND, H., ANDREBE, Y., BLANCHARD, P., et al., "New capabilities of the incoherent Thomson scattering diagnostics in the TCV tokamak: divertor and real-time measurements", *J. Instrum.* **14** 09 (2019) C09013–C09013.
- [19] PEREK, A., VIJVERS, W. A. J., ANDREBE, Y., et al., "MANTIS: A real-time quantitative multispectral imaging system for fusion plasmas", *Rev. Sci. Instrum.* **90** 12 (2019) 123514.
- [20] REIMERDES, H., DUVAL, B., ELAIAN, H., et al., "Initial TCV operation with a baffled divertor", *Nucl. Fusion*, **61** 2 (2021) 024002.
- [21] FÉVRIER, O., REIMERDES, H., THEILER, C., et al., "Divertor closure effects on the TCV boundary plasma", *Nucl. Mater. Energy*, **27** (2021) 100977.
- [22] ITER PHYSICS EXPERT GROUP ON CONFINEMENT AND TRANSPORT, ITER PHYSICS EXPERT GROUP ON CONFINEMENT MODELLING AND DATABASE, and ITER PHYSICS BASIS EDITORS, "Chapter 2: Plasma confinement and transport", *Nucl. Fusion*, **39** 12 (1999) 2175.
- [23] FAITSCH, M., MAURIZIO, R., GALLO, A., et al., "Dependence of the L-Mode scrape-off layer power fall-off length on the upper triangularity in TCV", *Plasma Phys. Controlled Fusion*, **60** 4 (2018) 045010.
- [24] HARRISON, J., VIJVERS, W., THEILER, C., et al., "Detachment evolution on the TCV tokamak", *Nucl. Mater. Energy*, **12** (2017) 1071–1076.
- [25] FÉVRIER, O., THEILER, C., HARRISON, J. R., et al., "Nitrogen-seeded divertor detachment in TCV L-mode plasmas", *Plasma Phys. Controlled Fusion*, **62** 3 (2020) 035017.